

Bulk and microscale compressive behavior of a Zr-based metallic glass

Y.H. Lai,^a C.J. Lee,^a Y.T. Cheng,^a H.S. Chou,^a H.M. Chen,^a X.H. Du,^{a,b} C.I. Chang,^a J.C. Huang,^{a,*} S.R. Jian,^c J.S.C. Jang^c and T.G. Nieh^d

^a*Institute of Materials Science and Engineering, Center for Nanoscience and Nanotechnology, National Sun Yat-Sen University, Kaohsiung 804, Taiwan, ROC*

^b*Department of Materials Engineering, Shenyang Institute of Aeronautical Engineering, Shenyang 110034, PR China*

^c*Department of Materials Science and Engineering, I-Shou University, Kaohsiung 840, Taiwan, ROC*

^d*Department of Materials Science and Engineering, The University of Tennessee, Knoxville, TN 37996-2200, USA*

Received 7 December 2007; revised 22 December 2007; accepted 5 January 2008

Available online 12 January 2008

Micropillars with diameters of 3.8, 1 and 0.7 μm were fabricated from a two-phase Zr-based metallic glass using focus ion beam (FIB), and then tested in compression at strain rates from 1×10^{-4} to $1 \times 10^{-2} \text{ s}^{-1}$. The apparent yield strength of the micropillars ranges from 1992 to 2972 MPa, or 25–86% increase over that of the bulk specimens. This strength increase can be rationalized by the Weibull statistics for brittle materials.

© 2008 Acta Materialia Inc. Published by Elsevier Ltd. All rights reserved.

Keywords: Metallic glasses; Micropillars; Compression test; Shear bands

Over the past decades, bulk metallic glasses (BMGs) have attracted extensive interest because of their unique properties such as good corrosion resistance, a large elastic limit, as well as high strength and hardness. However, the high strength of BMGs is often accompanied by a virtually zero plastic strain in tension and limited plasticity in compression. The brittleness problem severely impedes further exploitation of this material. To overcome this problem, many researchers made attempts to develop an extrinsic composite microstructure within the glassy matrix [1–4], or an intrinsic structure, such as dual-phase BMGs or in situ precipitated nanocrystals [5–8]. The basic idea is effectively to block or hinder the propagation of shear bands during deformation. For example, we have developed a phase-separated ductile Zr–Ni–Cu–Al BMG, exhibiting high compression ductility more than 30% [8].

Recently, metallic glasses are seen as the potential material for imprinting, molding and microelectromechanical systems (MEMs) because of their high strength, hardness, and processing flexibility in the supercooled liquid region. Thus, intense efforts have been made to

study the properties of small-sized samples. For example, it has been found that the strength of the face-centered cubic (fcc) single crystals such as Ni and Au [9,10] are a strong function of the specimen size in the micrometer range. This dramatic effect was proposed to be a result of the reduced specimen size which is smaller than the characteristic length for dislocation multiplication, resulting in dislocation starvation. In contrast, the BMG pillars do not deform by dislocation-mitigated processes [11,12]; instead, the plastic deformation in BMGs at room temperature is highly localized within shear bands or shear transformation zones (STZs) [13–15]. Our previous study on the brittle Mg–Cu–Gd-based glasses (no plastic compression strain in the bulk specimens) in the form of micropillars measuring 3.8 and 1 μm in showed a sudden strain burst, manifested as a constant flow stress, and no work-hardening [16]. Every strain burst event, regardless of the strain rate, proceeds within about one second, suggesting the strain rate during these bursts was at least 10^{-1} s^{-1} . There were very few shear bands, especially in the 1 μm pillar sample at a low strain rate: only one single shear band was present. It is thus of interest to examine the shear banding behavior of a much more ductile phase-separated Zr-based glass micropillars.

* Corresponding author. Tel.: +886 7 5252000; fax: +886 7 5254099; e-mail: jacobc@mail.nsysu.edu.tw

A ductile two-phase $Zr_{63.8}Ni_{16.2}Cu_{15}Al_5$ (in at.%) BMG was used in the current investigation due to its remarkable mechanical properties in the bulk form [8]. The cylindrical micropillars with a diameter of 3.8, 1.0, and 0.7 μm are fabricated using the FIB milling. The Zr-based BMGs were prepared by injection-casting into a water-cooled Cu mold with an internal cylindrical-shaped cavity of 2 mm in diameter. Detailed description of the casting methods have been described elsewhere [8]. The 2 mm BMG rods were sliced into disks of 1.5 mm in height by diamond cut, and then were ground with SiC paper from #1200 to #1400. Finally, the disk surface was polished to mirror finish with a diamond polishing paste, from 1 μm grit to 0.25 μm , prior to the FIB machining.

The microcompression samples were prepared using the dual focus ion beam system (FIB) of Seiko, SMI3050 SE, following the method developed by Uchic and Dimiduk [17]. A Ga beam operated at 30 keV and 7–12 nA was initially directed perpendicular to the surface of the BMG disk to mill a crater with a much bigger size (around five times of the corresponding pillar) island located in the center. Then, the same voltage and smaller currents of 0.7–0.09 nA were used to refine the preserved island in the center to a desired diameter and height of the pillar. A series of concentric-circle patterns were utilized to machine the pillars. The diameter, d , of a pillar, e.g., the 3.8, 1 and 0.7 μm in this paper, is referred to the diameter at the half-height position. However, due to slight tapered shape and the first initiation of shear banding at the top surface [16], all engineering flow stresses were calculated using the diameter of the top surface.

Microcompression tests were performed in an MTS nanoindenter XP with the continuous stiffness measurement mode using a flat punch indenter with an equilateral triangle cross-section measuring 13.5 μm in side length, which was also machined by FIB. These specimens were deformed in a prescribed displacement. The corresponding strain rates vary from 1×10^{-4} to $1 \times 10^{-2} \text{ s}^{-1}$. The data reported below are all engineering stresses and strains.

The micro-compression pillar samples have an approximate height-to-diameter ratio of 1:2.5, and the taper angle from the top to the bottom is about 2–3°. The morphologies of representative micropillars after compression are shown in Figures 1–3. The deformation mode of these micropillars is invariably the localized shear banding, independent of the specimen size. The first shear band is initiated from the corner of the contact surface between the specimen and compression indenter punch, where the sample has the least cross-sectional area and thus experiences the maximum stress.

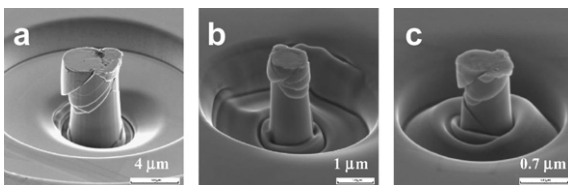


Figure 1. SEM micrographs showing the appearance of deformed pillars at a strain rate of $1 \times 10^{-4} \text{ s}^{-1}$: (a) 3.8 μm , (b) 1 μm , and (c) 700 nm.

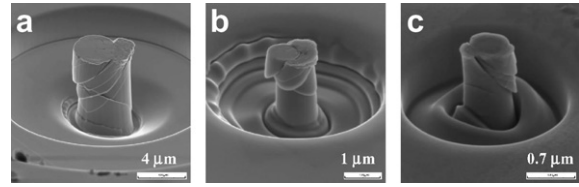


Figure 2. SEM micrographs showing the appearance of deformed pillars at a strain rate of $1 \times 10^{-3} \text{ s}^{-1}$: (a) 3.8 μm , (b) 1 μm , and (c) 700 nm.

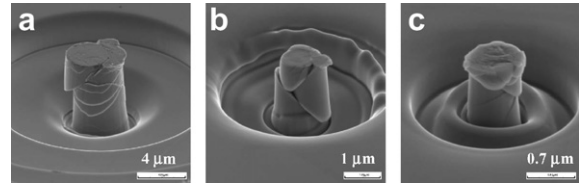


Figure 3. SEM micrographs showing the appearance of deformed pillars at a strain rate of $1 \times 10^{-2} \text{ s}^{-1}$: (a) 3.8 μm , (b) 1 μm , and (c) 700 nm.

With increasing straining, additional shear bands are triggered continually. From Figures 1–3 we can observe that sample shear-off does not occur immediately. This phenomenon is also reflected in the engineering stress–strain curves presented in Figures 4a–c.

It is pointed out that an engineering stress–strain curve is normally converted from the load–displacement data under the assumption that the specimen is uniformly deformed. In this study, the deformation of Zr-based BMG micropillars is dominated by the emission of shear bands in a manner of “strain burst” to release the energy, similar to that in crystalline solids [9]. However, in contrast to that in the case of Mg-based BMG micropillar which exhibits only one single strain burst (Fig. 4d), strain bursts in the present ductile Zr-based glassy micropillars are multiple and they appear to proceed in a progressive fashion. The increment of the load or the transformed engineering stress in each step varies from 100 to

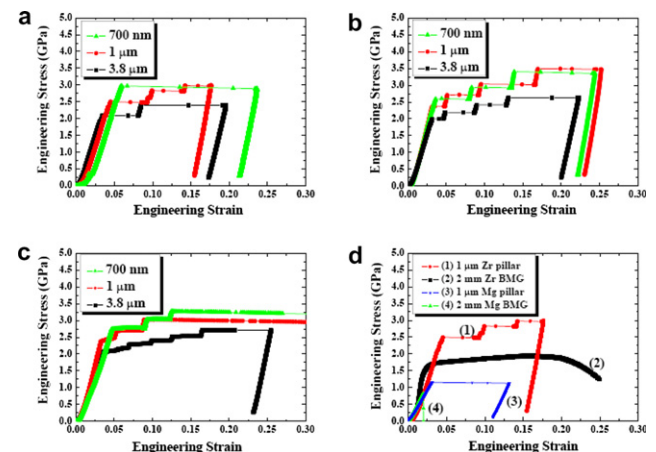


Figure 4. The micro-compression engineering stress–strain curves of the 3.8 μm , 1 μm and 700 nm micropillars at different strain rates of (a) $1 \times 10^{-4} \text{ s}^{-1}$, (b) $1 \times 10^{-3} \text{ s}^{-1}$, and (c) $1 \times 10^{-2} \text{ s}^{-1}$. The comparison of the curves for the Zr and Mg 2 mm bulk compression specimens, and the 1 μm Zr and Mg micropillars, compressed at 10^{-4} s^{-1} is presented in (d).

500 MPa, which cannot be considered to be negligible. There seems to be a blocking resistance for the propagating shear band. This seems to induce the initiation of the next shear band operative at a higher load or stress. In our parallel study on the 2 mm bulk Zr BMGs [8,18], multiple shear banding along various orientations was overwhelming and the engineering stress–strain curve (as also compared in Fig. 4d) shows extended ductility.

A close examination of Figs. 1–3 show that the number of shear bands in the current ductile Zr glassy micropillars (mostly 3–6) is much higher than that previously observed in the brittle Mg-based glassy micropillars (mostly 1–3) [16]. There appears to be a one-to-one correspondence between the number of shear bands (Figs. 1–3) and the number of stress jumps (Fig. 4), suggesting each stress jump is a result of the emission of a new shear band. Note also that the number of shear bands (Figs. 1–3), as well as the number of strain bursts (Fig. 4), appears to reduce with decreasing pillar size and decreasing strain rate. In fact, for the smallest 700 nm Zr-BMG pillars deformed at $1 \times 10^{-4} \text{ s}^{-1}$, there is only one displacement burst, resembling that seen in a brittle Mg-BMG micropillar [16]. Since both micropillars have a similar geometry, i.e. similar aspect ratio and taper angle, the increase in the number of strain bursts (or shear bands) is indicative of intrinsic plasticity in the Zr-based BMG. The current finding from the micropillars is consistent with that observed from the bulk specimens; namely, the Zr-based BMG is more ductile than the Mg-based BMG.

Despite the fact that the Zr-BMG micropillars are inhomogeneously deformed by localized shear bands, it is evident that the strength of these micropillars is a function of specimen size. If we take the first strain burst as the onset of plasticity, and assign it as the yield strength of the micropillar, the trend of increasing strength with decreasing specimen size becomes apparent. For example, at the intermediate strain rate of $1 \times 10^{-4} \text{ s}^{-1}$, the yield strengths of the 3.8 μm , 1 μm , and 700 nm pillars are 2088, 2496, and 2972 MPa, respectively. These values are all higher than the $1600 \pm 50 \text{ MPa}$ for the 2 mm $\text{Zr}_{63.8}\text{Ni}_{16.2}\text{Cu}_{15}\text{Al}_5$ bulk compression samples. These data are listed in Table 1. The highest yield strength recorded for the present Zr-based micropillar approaches 3000 MPa, which is more than 1.8 times the bulk value. The strain rate effect is, however, inconclusive and needs further investigation.

The measured elastic modulus was estimated from the elastic region of load and displacement curves, following the method developed by Lee et al. [16]. The data are also included in Table 1. After the correction of 1.25 for the extracted elastic modulus on the base of the finite element simulation of microcompression [19], the elastic modulus data varied around $78 \pm 6 \text{ GPa}$, which are

about the same as the data reported in literature for the Zr–Ni–Cu–Al BMGs ($\sim 80 \text{ GPa}$) [20]. The results on the elastic modulus indirectly indicate that the misalignment artifact on the yield stress measurement was minimized in this study.

The significant increase in the strength of the micropillar specimens might arise debate on the origins. There have been discussions on the possible causes for the observed stress increment [10,21]. One of them is the taper shape, and the other is the strengthening artifact caused by the FIB damaged layers. The former caused has been discussed and ruled out in our previous paper [16]. Here, we examine the effect of FIB damage, in particular the lateral thickness of the damage layers on the micropillar samples caused by FIB machining.

Bei et al. [22] have examined the hardening of the FIB-milled Mo single crystal caused by using various FIB beam voltage (5–30 kV), current (1.4–7 nA) and time (7.8–39 min). The acceleration voltage determines the depth of Ga ion penetration and the current and time determine the degree of damage in the damage zone. From the results of Bei et al., as long as the beam energy, or voltage times current, is lower than 30 kV nA, the hardness increment is less than 25%. In the current study, a FIB beam voltage of 30 kV is used, but coupled with a lower beam current, from the initial current 12 nA for rough beam milling for make the outer crater, progressively lowered to 0.7 nA for milling the pillar, and finally to 0.09 nA in the final trimming step. For the later critical stage, the beam energy is limited within 3 kV nA, well below the threshold value. Also noted is the fact that FIB used for the later stage trimming of our samples is directed parallel to the pillar side wall. Therefore, the FIB ion dose damage is expected to be even lower than the case of when the beam is bombarded perpendicular to the specimen flat surface.

To evaluate the FIB damage, Auger electron spectroscopy (AES, JEOL, JAMP-9500F) was employed for estimating the thickness of the FIB damaged layer in the Zr-BMG micropillar with a diameter of 3.8 μm . The Auger depth profile is shown in Figure 5. Ga signal levels off (the baseline intensity) at a depth of approximately 4 nm, indicating the thickness of FIB damaged layer is about 3–4 nm. This value is much lower than the damage thickness of 10–50 nm reported in crystalline Si [23,24]. Based on the current result, area contribution of the damage layer to the strength of a 700 nm-diameter micropillar is estimated to be only 3%, which is considered to be insignificant.

As discussed first by Schuster et al. [12] and later by Wu et al. [25] and Lee et al. [16], the strength increase with decreasing sample size can be rationalized by the Weibull statistics. For brittle materials, the variability of their strength is expected to be based on their flaw sensitivity

Table 1. Summary of the compressive stress/elastic modulus of $\text{Zr}_{63.8}\text{Ni}_{16.2}\text{Cu}_{15}\text{Al}_5$ glass at different strain rates

Sample size	$\dot{\epsilon} \sim 1 \times 10^{-4} \text{ s}^{-1}$	$\dot{\epsilon} \sim 1 \times 10^{-3} \text{ s}^{-1}$	$\dot{\epsilon} \sim 1 \times 10^{-2} \text{ s}^{-1}$
Bulk 2 mm	1600 MPa/80–90 GPa	1712 MPa/–	1847 MPa/–
3.8 μm	2088 MPa/77 GPa	1992 MPa/80 GPa	2054 MPa/79 GPa
1 μm	2496 MPa/63 GPa	2357 MPa/81 GPa	2365 MPa/85 GPa
700 nm	2972 MPa/81 GPa	2590 MPa/88 GPa	2733 MPa/72 GPa

All data are subject to a maximum 5% scattering.

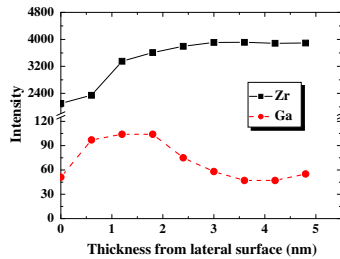


Figure 5. AES depth profile of the FIB milled Zr-based glassy micropillar with a diameter of 3.8 μm .

and can be analyzed using the Weibull statistics. The Weibull equation describes the fracture probability P_f as a function of a given uniaxial stress σ in the form of [26]

$$P_f = 1 - \exp \left[-V \left(\frac{\sigma - \sigma_u}{\sigma_0} \right)^m \right] \quad (1)$$

where σ_0 is a scaling parameter, m is the Weibull modulus, and V is the volume of the tested sample. The parameter σ_u denotes the stress at which there is zero failure probability, and is usually taken to be zero.

Using data listed in Table 1, and $V \propto d^3$, where d is the diameter of the pillar, the Weibull modulus is calculated to be around 60, as shown in Figure 6. This modulus value falls between the values for ductile alloys (~ 100) and brittle ceramics (~ 5) [27]. It is also within the range of the m values recently reported for the malleable $\text{Zr}_{48}\text{Cu}_{45}\text{Al}_7$ ($m = 73.4$) [25] and brittle $(\text{Zr}_{48}\text{Cu}_{45}\text{Al}_7)_{98}\text{Y}_2$ ($m = 25.5$) [25] and our Mg-based BMG ($m = 35$) [16]. Therefore, an increase in strength with decreasing sample size appears to be a result of reducing the population of critical flaw in test samples. The higher m -value of the current phase-separated ductile Zr BMGs than the more brittle Mg-based ones is also consistent with the general trend for Weibull modulus.

In conclusion, micropillars with diameters of 3.8, 1 and 0.7 μm were fabricated from a two-phase Zr-based metallic glass using focus ion beam (FIB), and then tested in micro-compression at strain rates from 1×10^{-4} to $1 \times 10^{-2} \text{ s}^{-1}$. The surface damage caused by FIB machining is about 4 nm thick, which has an insignificant effect on the subsequent mechanical properties. At all sizes, the plastic flow is localized in shear bands and manifested as strain bursts to release the energy. There are more shear bands in the Zr-based BMG as compared to that in Mg-based BMG, which is consistent with the fact that Zr-based BMG is more ductile than Mg-based BMG. The apparent yield strength of

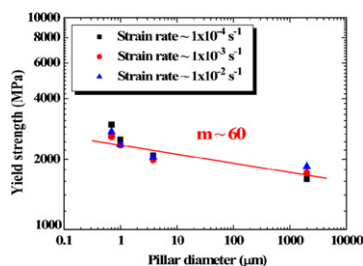


Figure 6. The strength–sample size relationship for the $\text{Zr}_{63.8}\text{Ni}_{16.2}\text{Cu}_{15}\text{Al}_5$ glassy specimens with different pillar diameters from 2 mm down to 700 nm.

the Zr-BMG micropillars is 1992–2972 MPa, which shows a 25–86% increase over that of the bulk specimens. The strength increase was successfully modeled using Weibull statistics for brittle materials. Thus, the increase in strength is a result of the fact that a smaller sample has a less defect population.

The authors acknowledge the sponsorship from National Science Council of Taiwan, ROC, under Project No. NSC 96-2218-E-110-001. This work was also supported by Division of Materials Science and Engineering, Office of Basic Energy Science, US Department of Energy under Contrast No. DE-FG02-06ER46338 with the University of Tennessee. The discussions on alloy design with Prof. K.C. Hsieh of National Sun Yat-Sen University and P.K. Liaw of the University of Tennessee are gratefully acknowledged.

- [1] C.C. Hays, C.P. Kim, W.L. Johnson, *Phys. Revs. Lett.* 84 (2000) 2901.
- [2] L.-Q. Xing, Y. Li, K.T. Ramesh, J. Li, T.C. Hufnagel, *Phys. Rev. B* 64 (2001) R180201.
- [3] A. Inoue, W. Zhang, T. Tsurui, A.R. Yavari, A.L. Greer, *Philos. Mag. Lett.* 85 (2005) 221.
- [4] Y.-K. Xu, H. Ma, J. Xu, E. Ma, *Acta Mater.* 53 (2005) 1857.
- [5] A. Inoue, T. Zhang, Y.H. Kim, *Mater. Trans., JIM* 38 (1997) 749.
- [6] K.F. Yao, F. Ruan, Y.Q. Yang, N. Chen, *Appl. Phys. Lett.* 88 (2006) 122106.
- [7] E.S. Park, D.H. Kim, *Acta Mater.* 54 (2006) 2597.
- [8] X.H. Du, J.C. Huang, K.C. Hsieh, Y.H. Lai, H.M. Chen, J.S.C. Jang, P.K. Liaw, *Appl. Phys. Lett.* 91 (2007) 131901.
- [9] M.D. Uchic, D.M. Dimiduk, J.N. Florando, W.D. Nix, *Science* 305 (2004) 986.
- [10] C.A. Volkert, E.T. Lilleodden, *Philos. Mag.* 86 (2006) 5567.
- [11] Q. Zheng, S. Cheng, J.H. Strader, E. Ma, J. Xu, *Scripta Mater.* 56 (2007) 161.
- [12] B.E. Schuster, Q. Wei, M.H. Ervin, S.O. Hruszkewycz, M.K. Miller, T.C. Hufnagel, K.T. Ramesh, *Scripta Mater.* 57 (2007) 517.
- [13] F. Spaepen, *Acta Metall.* 25 (1977) 407.
- [14] A.S. Argon, *Acta Metall.* 27 (1979) 47.
- [15] C.A. Schuh, T.C. Hufnagel, U. Ramamurty, *Acta Mater.* 55 (2007) 4067.
- [16] C.J. Lee, J.C. Huang, T.G. Nieh, *Appl. Phys. Lett.* 91 (2007) 161913.
- [17] M.D. Uchic, D.M. Dimiduk, *Mater. Sci. Eng., A* 400-401 (2005) 268.
- [18] X.H. Du, J.C. Huang, J.S.C. Jang, K.C. Hsieh, P.K. Liaw, Y.H. Lai, H.M. Chen, H.S. Chou, submitted for publication.
- [19] H. Zhang, B.E. Schuster, Q. Wei, K.T. Ramesh, *Scripta Mater.* 54 (2006) 181.
- [20] Y.H. Liu, G. Wang, R.J. Wang, D.Q. Zhao, M.X. Pan, W.H. Wang, *Science* 315 (2007) 1385.
- [21] J.R. Greer, W.C. Oliver, W.D. Nix, *Acta Mater.* 53 (2005) 1821.
- [22] H. Bei, S. Shim, M.K. Miller, G.M. Pharr, E.P. George, *Appl. Phys. Lett.* 91 (2007) 111915.
- [23] K. Thomposon, D. Lawrence, D.J. Larson, J.D. Olson, T.F. Kelly, B. Gorman, *Ultramicroscopy* 107 (2007) 131.
- [24] M. Fukuda, S. Tomimatsu, K. Nakamura, M. Koguchi, H. Shichi, K. Umemura, *J. Electron Microsc.* 53 (5) (2004) 479.
- [25] W.F. Wu, Y. Li, C.A. Schuh, *Philos. Mag.* 88 (2008) 71.
- [26] W.J. Weibull, *J. Appl. Mech.* 18 (1951) 293.
- [27] D.R. Askeland, *Science and Engineering of Materials*, PWS Publishing, Boston, 1994, p. 152.